Journal of Environmental Chemical Engineering 11 (2023) 109955

Contents lists available at ScienceDirect

Journal of Environmental Chemical Engineering

journal homepage: www.elsevier.com/locate/jece

Water decolorization and antifouling melioration of a novel PEBA1657/PES TFC membrane using chitosan-decorated graphene oxide fillers

Seyyedeh Rahil Mousavi [a], Morteza Asghari [a,b,*], Niyaz Mohammad Mahmoodi [c,**], Iman Salahshoori [a]

[a] Separation Processes Research Group (SPRG), Department of Chemical Engineering, University of Science and Technology of Mazandaran, Behshahr, Mazandaran, Iran
[b] UNESCO Chair on Coastal Geo-Hazard Analysis, Tehran, Iran
[c] Department of Environmental Research, Institute for Color Science and Technology, Tehran, Iran

ARTICLE INFO

Editor: Dong-Yeun Koh

Keywords:
Cationic dyes adsorption
Chitosan functionalized graphene oxide
Environmental pollutants
Thin film nanocomposite membrane
PEBAX®1657
Dye removal
Wastewater treatment

ABSTRACT

Novel chitosan-tailored graphene oxide (CSGO)-embedded poly(ether-*b*-amide) (PEBA) thin film nanocomposite (TFN) membranes have been fabricated and coated on ultraporous polyethersulfone. To synthesize the nature-friendly CSGOs, the covalent functionalization of GO has been done by carbohydrate polymer chitosan. The green nanofillers were then incorporated in the PEBA selective layer at different loadings up to 2 wt%. The structural studies were performed using FTIR, XRD, SEM, AFM and contact angle analyses, which confirmed the appropriate filler dispersion and enhanced hydrophilicity of the TFN membranes. Moreover, using nanofiltration (NF) for malachite green (MG) dye rejection, the effects of CSGO loadings, transmembrane pressure, feed concentration and duration on the membranes separation performance were also assessed. The membrane loaded with 0.1 wt% of CSGO showed the highest permeate flux, 3.2 times higher than that of the TFC membrane. The surface-decorated CSGO-filled TFN membranes also represented improved antifouling performance because the CSGO nanofillers had a positive charge due to the protonation of chitosan N-H groups in the acidic medium of this work.

1. Introduction

The water shortage problem is one of the most severe global issues attracting great attention since water is “the staff of life”. Due to rapid population growth, rational use of water resources, and water pollution, one of the grand challenges of modern societies is the depletion of water resources. Therefore, it is necessary to contemplate several approaches to exploit water resources, treat wastewater for reuse and obviate water pollution. Above all, wastewater treatment is extremely important due to its undeniable effects on the ecosystem ([15,28,39,55,78]; G.-d. [43]).

Undoubtedly, due to the presence of dangerous and toxic chemical compounds in industrial effluents, they are the most hazardous wastewaters threatening the environment and humankind [28]. Because of high water consumption during the processing operation in the textile industry, a large amount of highly-concentrated colored effluents are produced. Due to various dyes, surface active agents, oils, etc., in the discharged effluents of textile factories, their contribution to water pollution is reported as about 17–20%. Thereupon, treating their wastewater in order to attain the lowest possible concentration of pollutants is a very complicated and expensive task [15,32,41,53,58,62,86,87]. Furthermore, selecting an appropriate ment technique with simply-structured, cost-effective and more environmentally friendly properties is highly important. Membrane process as a well-set economic method has already been utilized in several applications such as desalination, hemodialysis, electrodialysis and filtrations [38]. As no chemical additives are required during the process, the membrane separation is expected to compete with and even go ahead of traditional approaches in other fields such as gas separation and wastewater treatment. Due to the determinative role of the membrane in such processes, it is necessary to investigate the performance of the semi-permeable barrier in terms of durability, stability (chemical, thermal

* Corresponding author at: Separation Processes Research Group (SPRG), Department of Chemical Engineering, University of Science and Technology of Mazandaran, Behshahr, Mazandaran, Iran.
** Corresponding author.
E-mail addresses: asghari@mazust.ac.ir, asgharimore@gmail.com (M. Asghari), mahmoodi@icrc.ac.ir (N.M. Mahmoodi).

https://doi.org/10.1016/j.jece.2023.109955
Received 24 November 2022; Received in revised form 25 February 2023; Accepted 16 April 2023
Available online 17 April 2023

Table 1
A summary of the recent research concerning GO-based TFN membranes for water treatment.

GO-based TFN membranes	Water treatment applications	Key findings	Year	Ref.
TiO_2 @GO-PA/PES	Desalination-cross-flow nanofiltration	Improved the hydrophilicity and roughness of the PA layer, improved water permeability and antifouling properties of the resulting TFN membrane	2017	(J.[84])
TiO_2 @rGO-PA/PSf	Desalination-reverse osmosis	Enhanced chlorine resistance by improving hydrophilicity, negative surface charge and the roughness of the PA layer, improved permeability, salt rejection and antifouling property	2015	Safarpour et al., ($year$) [69]
Zif-8 @GO-PA/PES	Salt removal and antimicrobial activity-cross-flow nanofiltration	Increased antimicrobial activity and salt retention, high hydrophilicity	2016	(J.[83])
GO-PA/PSf	Desalination-nanofiltration	Improved the hydrophilicity, water permeability, chlorine resistance and antifouling properties of the membrane, stability of TFN membranes in acidic and alkaline media	2016	(M. E.[5])
GO-PA/PSf	Desalination-reverse osmosis	Enhanced water permeation, anti-biofouling and chlorine resistance by tailoring the properties of the surface, such as hydrophilicity, roughness, charge and thickness	2015	Chae et al., ($year$) [17]
GO-PA/PSf	Desalination-cross-flow nanofiltration	Increased hydrophilicity, water permeability and salt rejection	2016	Yin et al., ($year$) [94]
GO-PA/PSf	Desalination-cross-flow nanofiltration	Enhanced hydrophilicity and negativity of the PA active layer, increased pure water flux, permeate flux and salt rejection	2016	Lai et al., ($year$) [52]
Sulfonated GO (SGO) @PA/PSf	Desalination-dead-end nanofiltration	Improved surface wettability, water flux, salt rejection, and antifouling properties	2019	(Y.[44])

and mechanical), permeability-selectivity (permeation flux-rejection) and antifouling specifications during separation [40,89].

The membrane effectiveness depends on two primary characteristics: permeability and selectivity. The membrane is more effective when these properties are higher. However, the permeability-selectivity trade-off is the major drawback of polymeric membranes, which confines their applications. Moreover, fouling the membrane surface and, consequently, flux decline is another undesirable phenomenon occurred during the ultrafiltration process. Therefore, hydrophilic polymeric membranes are considered as good candidates for water treatment. However, due to the higher chemical and thermal stability of many hydrophobic polymers, their application in the ultrafiltration process has been highlighted [61,92]. Thus, well-exploitation of a membrane water treatment is conditionally upon manipulating these polymeric membranes to improve their structure and physicochemical properties. It is achievable through the incorporation of nanomaterials, blending two polymers and fabrication of thin film composite (TFC) and/or thin-film nanocomposite (TFN) membranes [28,51,65,101]. Recently, the latter has been suggested as a leading solution to improve the performance of ultrafiltration membranes due to the simultaneous exploitation of favorable properties in two different polymeric structures.

In a TFC membrane, an ultrathin dense polymeric layer is commonly coated on a microporous sub-layer via different methods such as interfacial polymerization (IP), dip-coating, spin-coating, solution casting [22] and recently, co-casting [42] and pouring [1]. However, in some cases, a protective and a gutter layer might be used in the structure of TFC membranes [22]. In this class of membranes, the dense top-layer is mainly responsible for the operating performance of the membrane. In other words, a porous substrate transmits whatever is selected by this layer [22]. In the field of water treatment, a top-layer with high water permeation and antifouling properties is desired. Hereupon, the hydrophilicity of this layer has a significant effect on improving the abovementioned properties. One of the commercially reported polymers which can be recommended for this purpose is polyether block amide or PEBA. Actually, PEBA is a block copolymer comprised of rigid polyamide (PA) and soft polyether (PE) segments, and different categories of PEBA are available considering different types and compositions of these segments. As the hydrophilic functional groups of the etheric part seem to have the main contribution in PEBA hydrophilicity, the grades with higher PEO, such as 1657, 2533, 4011 and 1074, are favorable for water treatment. Although several works have been done in the field of PEBA-based TFC/TFN membranes for water treatment [20,61,68], dense morphology of PEBA makes it suitable for gas separation [11,13,25–27,45,46,56,57,59,6,67,7,77,8,9] and pervaporation ([19]; R. [47,64]) applications. Nowadays, with the aid of nanotechnology, it is thought that the same structure along with enhanced hydrophilicity, can create an ideal condition for water treatment. If an appropriate nanomaterial is embedded in the matrix of the TFC dense top-layer, a TFN membrane with improved properties will be attained. Indeed, a nanofiller improves the membrane performance by altering the physicochemical properties [15,93].

Graphene, a one-atom-thick sheet with a hexagonal pattern of sp^2-bonded carbon atoms, is a miracle of nanomaterials. Due to its intriguing properties, this promising carbon-based nanomaterial creates many opportunities for researchers in various fields, especially membrane-based applications for gas separation and water treatment ([2,12,18,51,79]; X. [85,90]; Y. [100]). Graphene, as a nanofiller, can be widely used to improve the structural and operational properties of the current polymeric membranes (Y. [44]; X. [85]). However, proper dispersion of the nanofillers in the polymer matrix is hardly achieved due to graphene agglomeration caused by strong Van-der-Waals forces among graphene layers [49]. As the most straightforward derivative of graphene, GO, with epoxide and hydroxyl functionalities on the basal plane and carboxyl ones on the edges, provides larger interlayer spacing and consequently, better dispersion than graphene. On the other hand, the intrinsic hydrophilicity of GO is a positive point for some gas separation and all water treatment membranes. Therefore, scientists open the door to using GO-based membranes in separation processes [10,13,66], especially, water purification processes in order to attain high water flux and antifouling properties ([33]; Y. [44,51,70,95]; Y. [100,102]). However, probable aggregation of GO at high concentrations results in opposite effects. To solve the agglomeration issue, one of the best choices is the chemical modification of GO with low-molecular-weight compounds, metal oxides, polymer chains and the other desirable

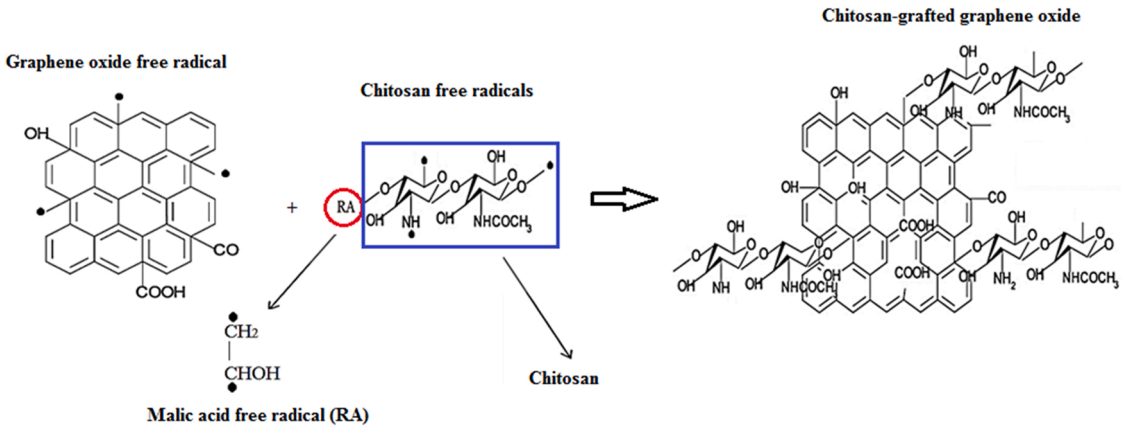

Fig. 1. The chemical reaction scheme to synthesize chitosan-aided surface decorated GO.

Table 2
Abbreviations of the prepared membranes.

Membrane abbreviation	Nanofiller loading (wt%)
TFC	-
TFNCSGO0.1	0.1
TFNCSGO0.5	0.5
TFNCSGO1	1
TFNCSGO2	2

functional groups ([36]; X. [85]). In Table 1, several studies of GO-based TFN membranes are summarized.

Polypyrrole polymer was also applied in our previous work for the surface decoration of GO nanosheets and dispersion engineering of fillers within PEBA mixed matrix membranes to enhance their CO_2 capture [13]. As reported, the selectivities and flux of the surface-decorated GO-filled membrane increased 50–60% and 10%, respectively.

Among different polymeric chains for functionalization and/or surface decoration, the carbohydrate polymer chitosan can be considered as a good candidate since it is a plenteous natural biopolymer with remarkable biological and economic features ([14,40]; V [96]; Vida [97]; V Z[98]; S. [99]). Furthermore, the amino-hydroxyl groups of chitosan award it a hydrophilic nature ([34,60,81]; E. [71,74]) which paves the way to achieve enhanced water permeation and antifouling properties. Therefore, scientists have recently tended to employ a chitosan/GO hybrid for synthesizing various composites [30,35,50,54,82], adsorbents [21,29,31] and membranes ([24,37]; H. [72,73,75,80,91]) in the field of water purification.

Our goal was to create a new mixed matrix structure that is environmentally friendly, well-dispersed, and has increased hydrophilicity to enhance water permeation and improve antifouling properties in membrane water treatment. Therefore, the carbohydrate polymer chitosan has been used for synthesizing surface-decorated graphene oxide nanosheets incorporated up to 2 wt% within the PEBA matrix to prepare well-dispersed mixed matrix selective layers of TFN membranes. Afterwards, an ultrathin layer of CSGO/PEBA was deposited on a porous PES sublayer. The synthesized TFN membranes were then analyzed in terms of chemical structure and morphology using SEM, AFM, FTIR, XRD and contact angle tests. Moreover, the separation performance was investigated through pure water flux (PWF) and Malachite green (MG) dye removal tests. In this purpose, a simple cross-flow nanofiltration set-up was used to pack a TFN membrane into a flat-sheet module.

2. Experimental

2.1. Materials

PEBAX®1657 copolymer (40 wt% PA6 and 60 wt% PEO), Chitosan (CS) biopolymer (with > 85% deacetylation degree and medium molecular weight) and Polyethersulfone polymer (with Mw=75,000 g/mol), were purchased from ARKEMA (France), Sigma-Aldrich (Germany) and BASF (Germany), respectively. Freeze-dried single-layer graphene oxide (GO) were obtained from Kara Pajuhesh Amirkabir Co., Iran. The employed solvents i.e. ethanol (EtOH, 96%) and dimethylacetamide (DMAc, 99.5%) were purchased from Merck and BASF Co., Germany, respectively. Potassium permanganate (KMnO4), sulfuric acid (H_2SO4) (98%) and malic acid, utilized in the GO functionalization process, were supplied from Merck (Germany).

2.2. Synthesis of chitosan-aided surface-decorated GO (CSGO)

A homogeneous dispersion of GO (0.1 g) in distilled water (DI, 10 mL) was obtained with the aid of an ultrasonic bath. The sonication process was carried out at room temperature for 3 h. The solution was then subjected to a reaction with 0.13 g of chitosan in the presence of KMnO4 (0.04 g), malic acid (0.06 g) and H_2SO_4 (0.75 mL). Indeed, potassium permanganate and malic acid were employed to produce the required free radicals in the reaction shown in Fig. 1 in detail. The reaction process was done under continuous stirring for 3 h at 58 °C. In order to remove impurities, the resultant solution was washed with acetone 4–5 times and let dry at ambient temperature for at least 24 h.

2.3. Preparation of TFN membrane

The pouring method was utilized to coat an ultrathin polymeric layer of PEBA on the porous surface of PES support. Furthermore, the PES support was prepared by the wet phase-inversion method. The procedure of fabricating bare PES and CSGO-PEBA/PES TFN membranes are voluminously explained as follows. At first, a polymeric dope consisting of PES (18 wt%), DMAc (80.2 wt%) and PVP (1.8 wt%) was prepared by slow-stirring at ambient temperature for 24 h. Then, the degassed solution was cast on a glass plate and immediately submerged in distilled water for solvent-nonsolvent exchange. In order to remove residual DMAc, the membrane films were placed in another water bath for a full day. Afterwards, the membranes were put between two pieces of filter paper and dried at ambient temperature for 24 h.

In order to prepare the top layer of polymeric dope, CSGO was dispersed in a 10 mL ethanol/water mixture (70:30 wt%) under an ultrasonic probe for 30 min until a homogeneous solution was gained. Simultaneously, 4 wt% PEBA was dissolved in the remaining solvent (~

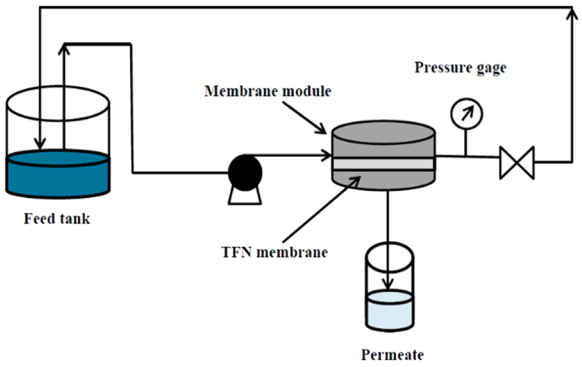

Fig. 2. Nanofiltration set-up.

10 mL) at 80 °C for 4 h. The abovementioned mixtures were mixed with each other under an ultrasonic bath at 80 °C for 1 h.

The final polymeric dope was stirred at 80 °C for 24 h. The polymeric dope of neat PEBA was prepared in the same way explained above without adding the nanofillers. After debubbling the dope, it was poured on PES support fixed on a glass plate with an angle of 60º. The as-prepared membranes were dried at ambient temperature for 24 h, followed by oven-drying (40 °C) for 24 h.

Due to different concentrations of CSGO in the synthesized membranes, the following abbreviations were considered to introduce a specific membrane, see Table 2.

2.4. Membrane characterization

Fourier-transform infrared (FT-IR) spectroscopy and X-ray diffraction (XRD) analyses were used to structurally evaluate the membrane samples and the synthesized nanomaterial. Hereof, an FT-IR spectrometer (in the range from 400 to 4000 cm^{-1}, PerkinElmer Spectrum One, US) was employed to indicate the functional groups, whereas the crystallinity of the samples was determined by the emerging peaks in their XRD patterns (Model: '''X'PertPro). Furthermore, atomic force microscopy (AFM, Model: dual scope, DME, Germany) was employed to investigate the membrane morphology and surface roughness. In order to assess the thickness and the morphology of the membrane layers, i.e. the selective layer and the support as well as the nanofillers' position on the membrane surface, scanning electron microscope (SEM and FESEM, Model: MIRA3, TESCAN, Czechia) analysis was utilized. A water contact angle test was also used to determine the hydrophilicity of the membranes (OCA15 plus instrument, sessile drop method).

2.5. Membrane performance

The performance of all synthesized TFC and TFN membranes were investigated quantitatively in terms of pure water flux (PWF), permeate

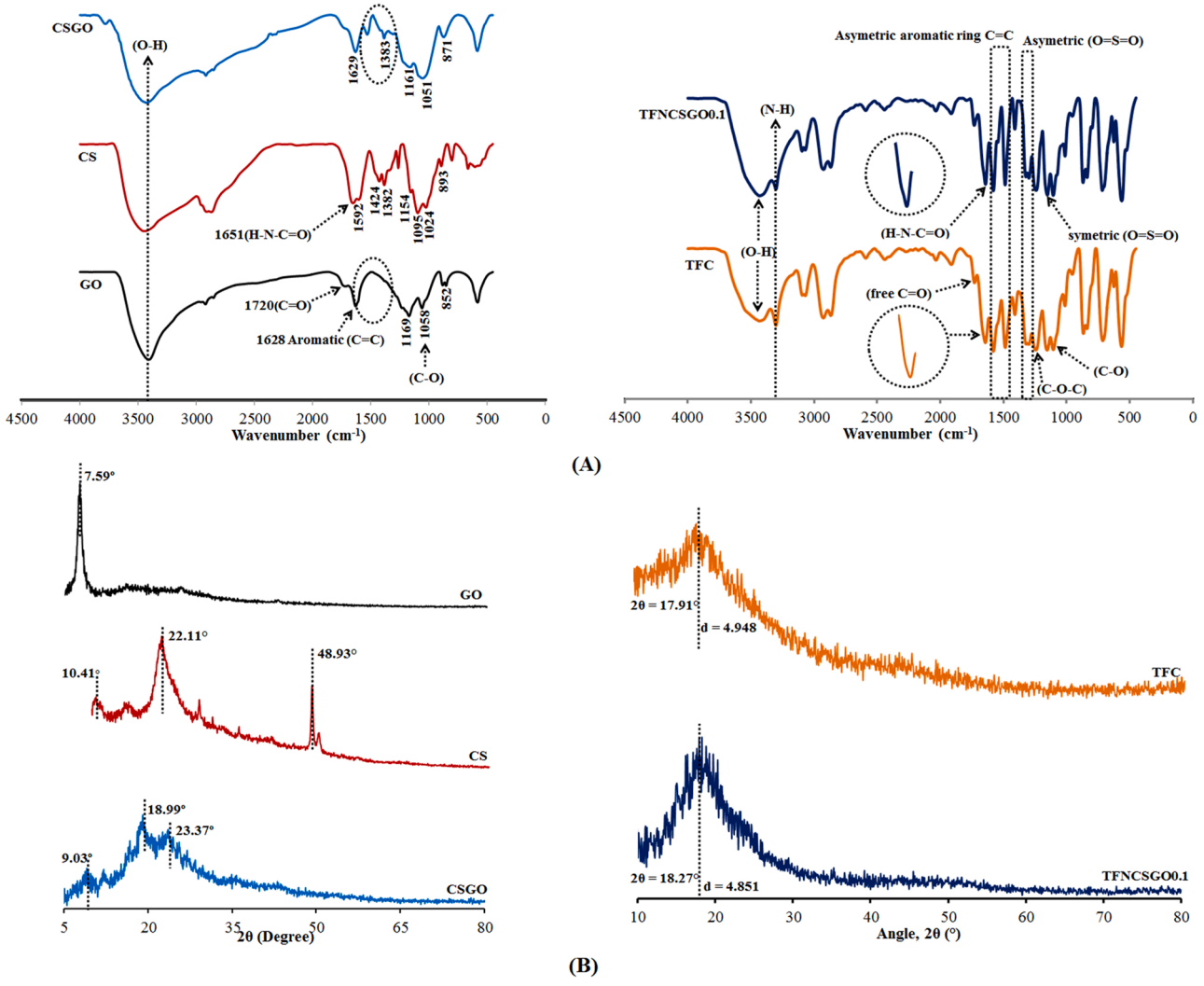

Fig. 3. (A) FTIR spectra and (B) XRD patterns of GO, CS, CSGO, TFC and TFNCSGO0.1.

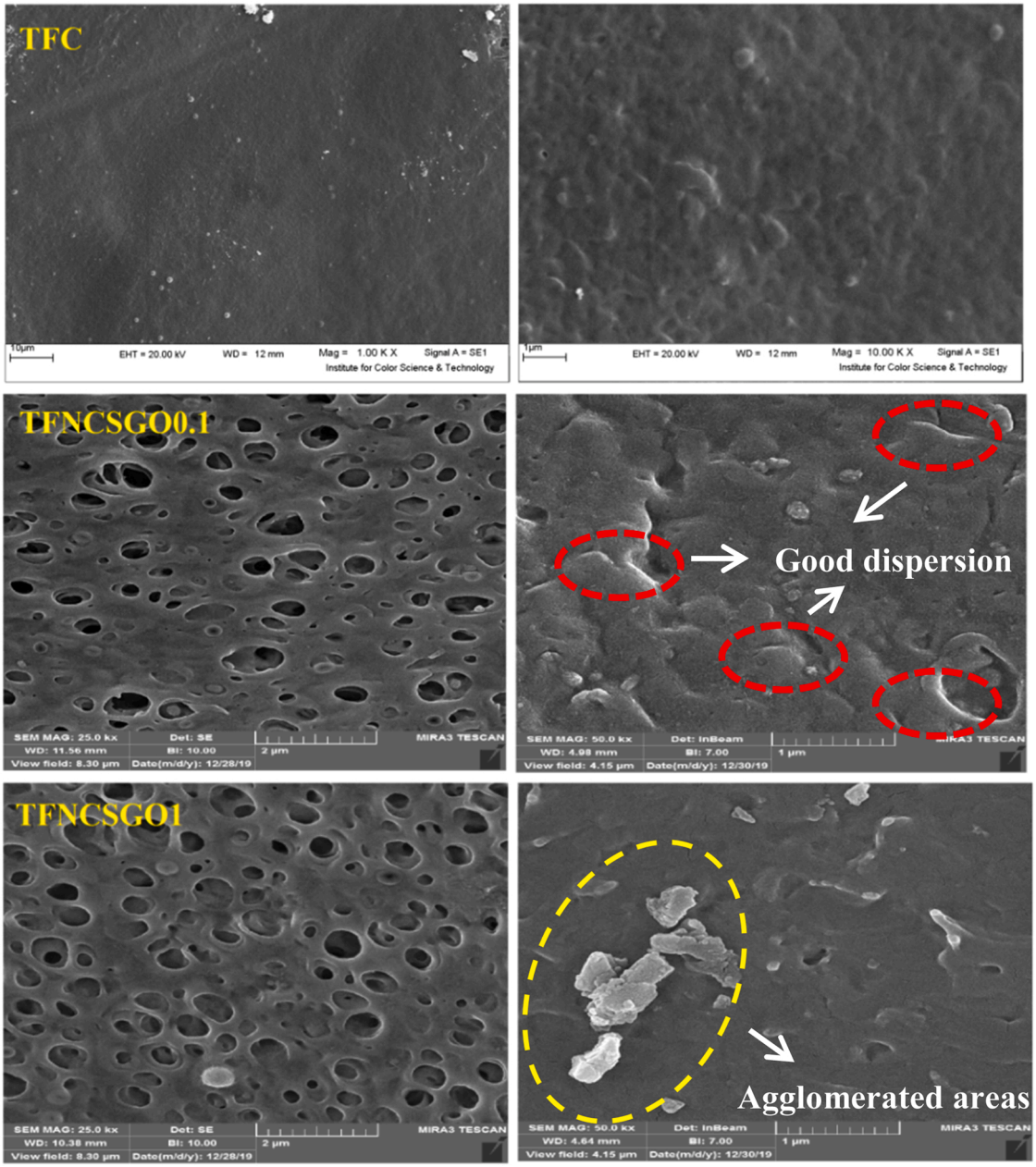

Fig. 4. FESEM images of TFC, TFNCSGO0.1 and TFNCSGO1 membranes.

flux and rejection. All experiments were handled in a cross-flow laboratory nanofiltration set-up with an effective area of 3.14 $cm^{2,}$ as shown in Fig. 2.

In order to investigate the pressure effect on the membrane performance, the PWFs of the membranes were calculated at three transmembrane pressures (1, 2 and 3 bar). Furthermore, the decolorization actions of the membranes were evaluated during a 300 min period of time in which the samples were collected per hour. In fact, the permeate flux and rejection changes were estimated versus time. All decolorization tests were done at 2 bar for two feed concentrations of malachite green (MG) dye (30 and 60 mg/L). Finally, the concentrations of the sample were estimated by the maximum wavelength of MG read from the ultraviolet spectrophotometer. To calculate the permeate flux and rejection of the membranes, Eqs. 1 and 2 were utilized, respectively:

$$J = V/A{\cdot}\Delta t \quad (1)$$

$$R\% = (1\text{-}C_p/C_f) \times 100\% \quad (2)$$

where, V, A, Δt, R, C_f and C_p are the permeate volume, effective membrane area, permeate time, rejection factor, feed and permeate concentrations, respectively.

3. Result and discussion

3.1. FTIR and XRD

In order to specify the surface functional groups in the structure of GO, CS, CSGO, TFC and TFNCSGO0.1, FTIR analyses are typically displayed in Fig. 3 A. Furthermore, their crystallinity assessed by the relative XRD patterns is presented in Fig. 3B. As shown in Fig. 3A, the obtained spectra of GO and CS are nearly the same as those in the literatures (F. A. A. [4,29,35,36,66]; Y. [100]). According to the FTIR curve of chitosan, the absorption peak at 3442 cm^{-1} represents the broad band of OH group vibration. Furthermore, the peaks at 1652 cm^{-1}, 1600 cm^{-1}, 1095 cm^{-1} and 2871 cm^{-1} introduce amide

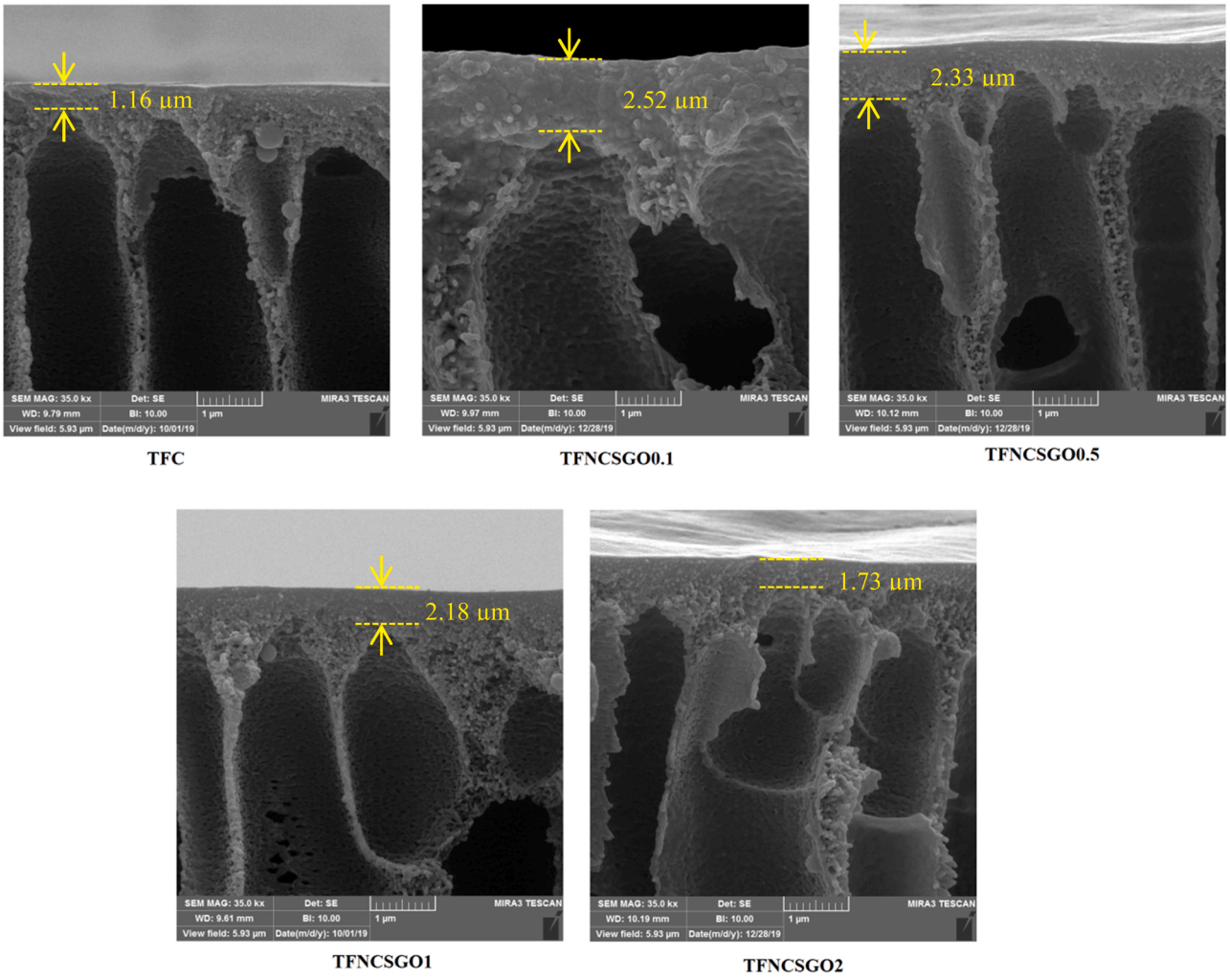

Fig. 5. Cross-sectional images of TFC, TFNCSGO0.1, TFNCSGO0.5, TFNCSGO1 and TFNCSGO2.

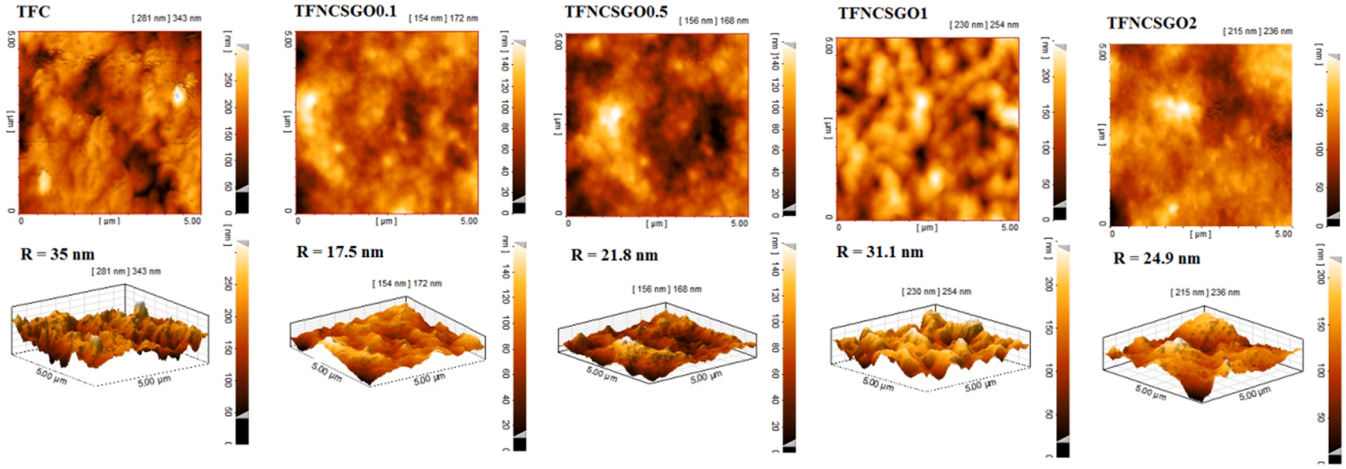

Fig. 6. 2 and 3D-AFM images of TFC, TFNCSGO0.1, TFNCSGO0.5, TFNCSGO1 and TFNCSGO2.

group vibration, protonated amine vibration, the vibration of CO groups and CH stretching vibration in CH_2 and CH_3, respectively.

In the GO spectrum, various oxygen-containing polar groups are distinguished, which are responsible for the high hydrophilicity of GO. These prominent characteristic peaks located at 3406 cm^{-1}, 1720 cm^{-1}, 1628 cm^{-1} and 1058 cm^{-1} correspond to the stretching vibrations of hydroxyl (-OH), carboxyl and carbonyl (C═O), aromatic C═C and alkoxy (C-O) functional groups, respectively. Due to the hydrogen bonding interaction between water molecules and the GO polar groups, this carbon-based nanomaterial is well-dispersed in water [54,76,88,102]. Similarly, several absorption peaks are distinguished in the CS biopolymer spectrum relating to specific functional groups. They are

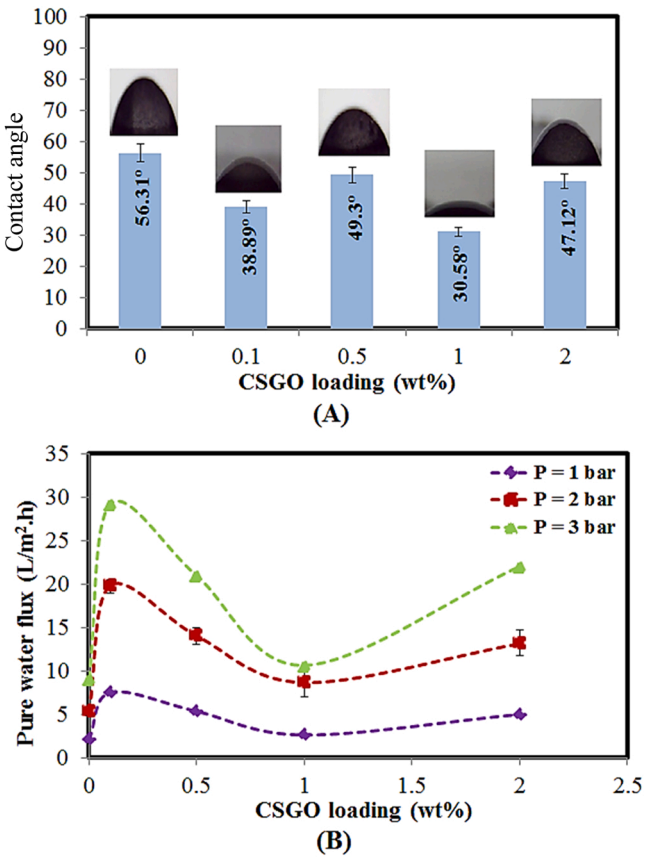

Fig. 7. (A) Surface contact angles (CA) and (B) Pure water fluxes (PWFs) of the TFC and TFN membranes versus CSGO loading.

3442 cm^{-1} (-OH vibration), 1651 cm^{-1} (amide group vibration), 1600 cm^{-1} (protonated amine vibration) and 1095 cm^{-1} (CO groups) [54]. Moreover, as illustrated in Fig. 3A, the obtained spectrum for the synthesized nanomaterial (CSGO) confirms CS grating on GO. Comparing its FTIR curve with those of raw materials (i.e. GO and CS), the peaks of GO and CS are recognizable as well as some new peaks.

The new peaks observed in the CSGO curve imply forming a chemical bond between CS and GO. The sites of the new peaks have been shown by an oval in the figure. For instance, the appearance of an absorption peak at 1529 cm^{-1} is related to the amides or carbamate esters formed during the grafting reaction.

The XRD patterns of GO, CS and CSGO are indicated in Fig. 3B. According to the figure, the characteristic peak of GO appeared at $2\theta = 7.59°$, suggesting highly-laminated GO structure, which is favorable in the synthesis of nanomaterials. Based on " 'Bragg's law ($d=\lambda/2\sin\theta$), the smaller 2θ describes the higher D-spacing, which in turn decreases the number of the stacked GO nanosheets [7].

Herein, the D-spacing of GO is higher than that in the kinds of literature i.e. 0.822 nm [66,94]. In contrast, to GO, the peaks that emerged at $2\theta = 9.03°$ and 18.99° describe smaller D-spacing and amorphous structure of CSGO. Indeed, due to the interaction of chitosan functional groups with those of GO, the number of the surface oxygen functional groups of GO decreases, resulting in lower single-layer GO nanosheets [35,94]. Furthermore, the amorphous structure of chitosan is confirmed by the characteristic peaks that emerged at $2\theta = 10.41°$ and 22.11° (Y. H. [48,90]).

According to the FTIR spectra of the TFC membrane, the characteristic peaks of PEBA are observed at 3302, 1643, 1729 and 1105 cm^{-1}. The first two wavenumbers introduce N-H and H-N-C═O groups in the hard segment of PEBA, i.e. polyamide (PA). The latter two ones which correlate to the soft PEO of PEBA, showing the ester C═O and the bonded -C-O- functional groups [23]. Additionally, the chemical structure of the PES substrate (see Fig. 1) is confirmed by the absorption peaks at 1480–1580, 1154 and 1332 cm^{-1} corresponding to asymmetric aromatic ring C═C, symmetric O═S═O and asymmetric O═S═O, respectively ([20]; J. [83]).

In the FTIR curve of TFNCSGO0.1, all of the absorption peaks in the TFC membrane are observed, demonstrating that the overall polymer structure has been retained. However, some little shifts to lower or higher values are observed and the intensity of some peaks has been changed. For example, the intensity of the C═O group (free and bonded) in the PA segment has been investigated. As observed in the TFC spectrum, the free C═O peak is not seen. Indeed, there are a few free C═O functional groups so that the bonded one covers the corresponding peak. In other words, the interchain hydrogen bonds between N-H and C═O groups in the PA part have been very strong, leading to phase separation [7]. According to the literatures, incorporating nanofillers into PEBA interrupts the interchain bonds within PA block, and the number of free C═O groups increases compared to PEBA. These free C═O groups

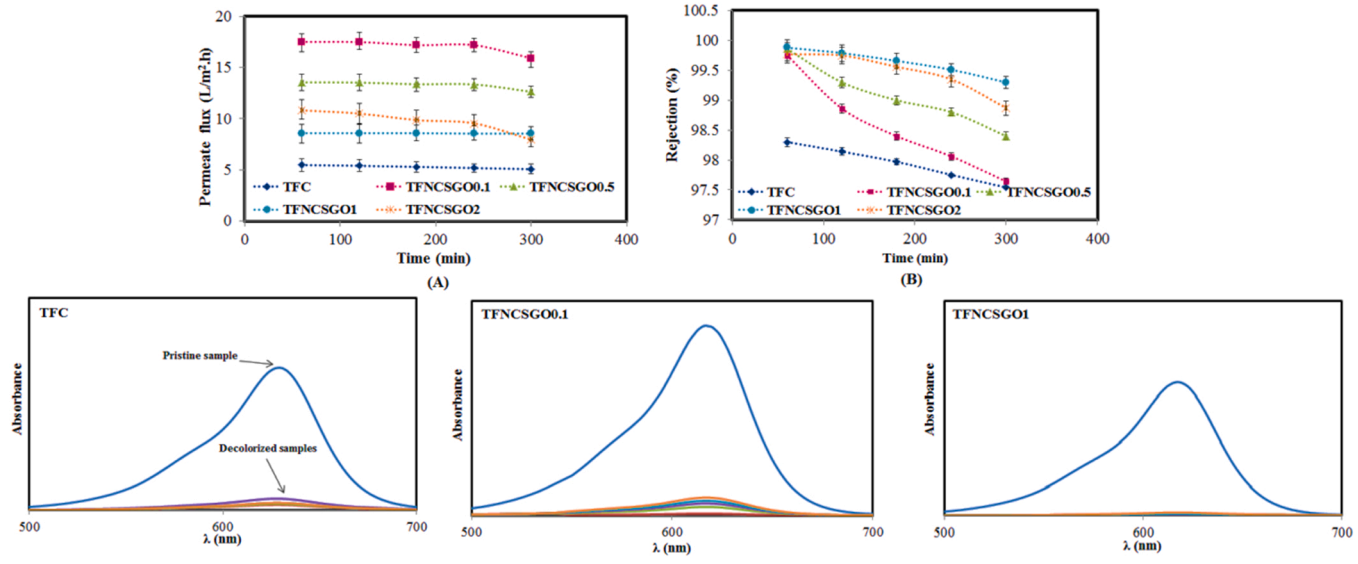

Fig. 8. Malachite green permeate flux (A) and rejection (B) of TFC and TFN membranes vs. time at 2 bar and the spectrophotometric graphs of TFC, TFNCSGO0.1 and TFNCSGO1 membranes.

Table 3
Nanofiltration performance of TFN membranes in this work and literatures.

Active layer/ sublayer	Nanofiller	Permeation flux (L/m^{2}h)	Rejection	Pressure (bar)	Ref.
PA/PES	**0.2wt%** TiO_2 @GO	22.43	Na_2SO_4 **98.8%**	4	(J. [84])
PA/PSf	**0.02wt%** TiO_2 @rGO	51.3	NaCl **99.45%**	15	Safarpour et al., ($year$) [69]
PA/PES	**0.2wt%** Zif-8 @GO	32.5	Na_2SO_4 **100%** $MgSO_4$ **77%**	8	(J. [83])
PA/PSf	**100mg/L** GO	29.6	NaCl ≥ **97%**	15	(M. E. [5])
PA/PSf	**38mg/L** GO	~ 16.7	NaCl **99.4%**	15.5	Chae et al., ($year$) [17]
PA/PSf	**0.015wt % GO**	~ 59.4	NaCl ~ **93.8%** Na_2SO_4 ~ **97.3%**	20.7	Yin et al., ($year$) [94]
PA/PSf	**0.3wt%** GO	> 14.4	Na_2SO_4 **95.2%** $MgSO_4$ **91.1%** $MgCl_2$ **62.1%** NaCl **59.5%**	8	Lai et al., ($year$) [52]
PA/PSf	**0.3wt%** SGO	11.8	Na_2SO_4 **96.45%**	4.96	(Y. [44])
PA/PES	**120mg/L** CS-GO	61.47	NaCl **95.56%**	14	Hegab et al., ($year$) [37]
PA/PES	**0.5wt%** GO-CS	21.34	NaCl **91.4%**	5	Du et al., ($year$) [24]
PEBA/ PES	**wt%** CSGO **1wt%** CSGO	17.068 8.58	Malachite green dye **98.54%** **99.63%**	2	This work

create new strong hydrogen bonds with the amine group of CS. Therefore, the bonded C═O absorption peak in TFNCSGO0.1 is sharper and greater than that of TFC, as highlighted in a circle in Fig. 3A.

As indicated in Fig. 3B, there are no sharp, strong peaks in the XRD patterns of the TFC and TFNCSGO0.1 membranes, which approve the semi-crystalline structure of PEBA. However, a more intense Bragg peak emerges in the XRD pattern of TFNCGO0.1 compared to that in TFC. Indeed, new interactions between CSGO and PEBA enhance the crystallinity of this segment. Furthermore, according to the patterns, the peak at $2\theta = 17.91^\circ$ is related to the crystalline part of PEBA that appeared by the hydrogen bonds in the PA segment. By incorporating 0.1 wt% CSGO nanofillers within the PEBA matrix, this peak is shifted to a higher value at $2\theta = 18.27^\circ$. Based on " 'Bragg's law, the interchain space (d-spacing) decreases from 4.948 Å for the TFC membrane to 4.851 Å for TFNCSGO0.1. This decreased d-spacing approves the strong and appropriate linkage between the CSGO and PEBA, as confirmed by FTIR. Moreover, any characteristic peak of CSGO is not observed in the XRD curve of TFNCSGO0.1, which suggests the presence of well-dispersed monolayer CSGO in the polymeric matrix [3,7,23].

3.2. FESEM

The surface FESEM images of TFC, TFNCSGO0.1 and TFNCSGO1 membranes are presented in Fig. 4. As observed, the surface morphology of the TFN membranes is not thoroughly different from that of TFC one. In fact, all the membranes show a dense defect-free skin layer. According to Fig. 4, the surface of the TFC membrane is homogeneous whereas bright spots on the surface of the TFN membranes indicate the existence of CSGO nanofillers. As seen in Fig. 4, for very small quantities up to 0.1 wt%, the CSGOs are well-incorporated within the polymer matrix. As a result, the number of knotted areas on the membrane surface decreases to its minimum value. Furthermore, the sites in red in Fig. 4 approve the appropriate interaction of the CSGO nanofillers with PEBA, as explained in detail in § 3.1. As observed, there is no gap between the nanofillers and the polymeric matrix. In other words, the existence of the PEO segment in the rubbery PEBA creates good adhesion between the nanofiller and PEBA [3].

On the other hand, the hydrophilic CSGOs decelerate the evaporating rate and, thus, the phase-inversion process. Therefore, a new integral skin layer structure with favorable morphology is formed [16,94]. Furthermore, the surface roughness (ups and downs) decreases, creating a surface with lower roughness, as observed in the 2D-AFM image. At higher CSGO loadings, the agglomeration of CSGO nanosheets results in the formation of nodules on the membrane surface [16,52,68,94]. Moreover, the lumps on the membrane surface defined in the image of TFNCSGO1 increase the surface roughness. These results are compatible with the corresponding AFM image, too.

The cross-sectional SEM images of the TFC, TFNCSGO0.1, TFNCSGO0.5, TFNCSGO1 and TFNCSGO2 are shown in Fig. 5. The figures show the porous structure of the PES substrate on which an

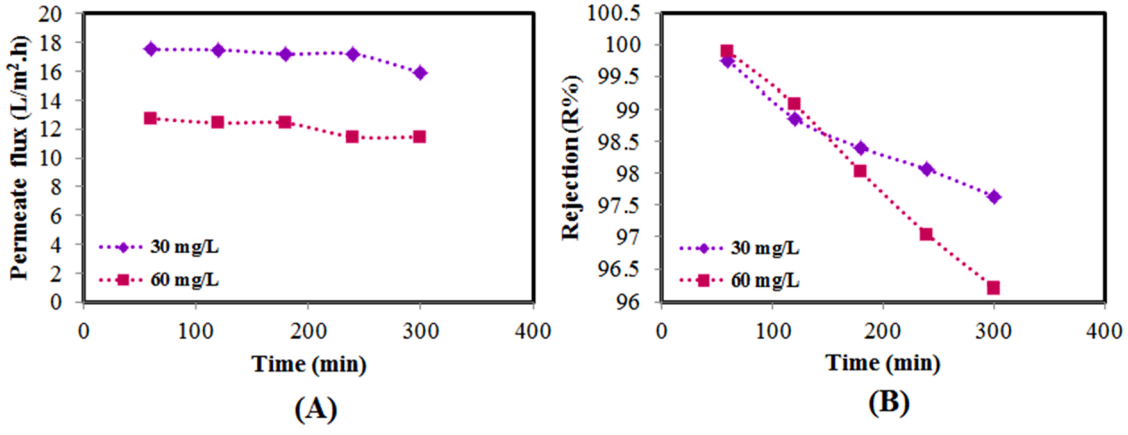

Fig. 9. The effect of feed concentration on the permeate flux (A) and rejection (B) of TFNCSGO0.1 vs. time at 2 bar.

ultrathin dense layer was deposited is clearly seen. As observed, the finger-like pores of PES provide favorable passways for water molecules (Y. [44,102]). Furthermore, a dense homogeneous and defect-free skin layer is observed in the cross-section images of both TFC and TFN membranes. Additionally, any gaps are not seen in the interface representing the excellent compatibility of PEBA/PES.

From Fig. 5, the thickness of the selective layer has increased from 1.16 μm for TFC to 2.52 μm for TFNCSGO0.1. The reason lies behind the effect of CSGO addition on the cohesive force in the PEBA solution and the adhesive one between the PES substrate and PEBA dope. Indeed, the hydrophilic CSGO nanofillers increase the cohesive force within the polymeric dope and cause less penetration in the substrate. Therefore, more deposition of the polymeric dope on PES occurs and the thickness of the TFNCSGO0.1 increases (Y. [44,52]). Adding more CSGOs increases the attraction among CSGOs, impressing the dispersion stability. Therefore, more CSGOs migrate to the surface (see AFM results, Fig. 6), and more PEBA absorbs into the substrate. As result, the active layer thickness decreases with CSGO loadings of more than 0.1 wt%.

3.3. AFM

Fig. 6 presents the 2 and 3D-AFM images of the TFC, TFNCSGO0.1, TFNCSGO0.5, TFNCSGO1 and TFNCSGO2. Furthermore, the average surface roughness of the membranes is reported as 35 nm, 17.5 nm, 21.8 nm, 31.1 nm and 24.9 nm for TFC, TFNCSGO0.1, TFNCSGO0.5, TFNCSGO1 and TFNCSGO2, respectively. Consistent with SEM images, the TFN membranes show smoother surfaces than TFC ones due to the presence of the hydrophilic CSGO nanofillers. According to 3D-surface images in Fig. 6, the least bumps and dents are seen for TFNCSGO0.1, representing its smooth surface.

This circumstance can be explained according to homogeneous dispersion and well accommodation of the CSGOs within PEBA at low dosages, as explained in § 3.2. By increasing CSGO to 1 wt%, some clusters form as a result of CSGO aggregation, thus increasing the surface roughness [102]. At percentages over 1 wt%, although there are more CSGOs on the surface, the average roughness decreases due to the large agglomerated areas on the surface.

3.4. Contact angle

All the water contact angle data determined for TFC and TFN membranes are the average values obtained for four random surface locations. The results are illustrated in Fig. 7(A). As presented, the contact angles are 56.31°, 38.89°, 49.3°, 30.58° and 47.12° for TFC, TFNCSGO0.1, TFNCSGO0.5, TFNCSGO1 and TFNCSGO2 membranes, respectively. The results indicate that all TFN membranes have lower contact angles and, consequently, higher hydrophilicity than TFC ones.

Indeed, the hydrophilic functional groups of CSGOs play a significant role in the enhanced hydrophilicity of the TFN membrane surfaces (M. E. [5,16,37]; Y. [44,69]). However, an authentic comment on the contact angle behavior involves considering important parameters like surface structure, surface roughness and nanofiller agglomeration ([16]; Y. [44]). As observed, the contact angle shows a descending-ascending trend with CSGO concentration. Based on " 'Wenzel's model described as $\cos\theta^* = r\cos\theta$, the surface contact angle of a hydrophilic rough surface ($r > 1$) is inversely correlated with its roughness. This trend is observed for the contact angle changes at CSGO dosages greater than 0.5 wt%. i.e. the surface roughness increases, and the surface contact angle decreases gradually, so the minimum contact angle is perceived at 1 wt% CSGO.

At higher loadings of CSGO (> 1 wt%), the average roughness decreases owing to the increased accumulation of CSGOs on the surface (Y. [44]). Accordingly, the contact angle increases from 30.58° for TFNCSGO1 to 47.11° for TFNCSGO2. However, at concentrations lower than 0.5 wt%, the inverse correlation between the abovementioned characteristics is not seen. This trend can be explained as follows. At low concentrations of CSGO (≤ 0.1 wt%), surface roughness and contact angle decline simultaneously. This is owing to the membrane surface's wettability increment caused by surface hydrophilicity increment ([17]; Y. [44,94]). Adding more CSGO to 0.5 wt% disrupts the well-dispersion of the nanofillers in the PEBA matrix and creates some agglomerated areas on the surface. Therefore, the TFNCSGO0.5 roughness increases in comparison to that of TFNCSGO0.1. Moreover, the interlayer spacing of the CSGO nanosheets reduces due to the stacking of the layers. This behavior increases contact angle by reducing the water transfer channels and thus, hydrophilicity.

3.5. Operating assessment of TFC/TFN membranes

In this part, the membrane's performances are investigated considering the effects of transmembrane pressure and nanofiller loading, process time and feed concentration.

3.5.1. Transmembrane pressure and nanofiller loading

Due to the noticeable role of pressure driving force in the membrane separation process, its effect on PWF was investigated at 1, 2 and 3 bar for all synthesized membranes. The experimental data are depicted in Fig. 7(B).

It is evident that the greater the driving force, the higher the mass flux. So, it is expected to have higher PWF at higher pressures. According to Fig. 7(B), the obtained results confirm the abovementioned comments. The same results are elsewhere in the literatures (M. E. [5,20,68]; J. [83]). Additionally, the effect of CSGO concentrations on the membrane permeation performances was evaluated. As shown, the PWFs of all TFN membranes are higher than that of the TFC one. It is due to the incorporation of CSGO nanosheets in the PEBA skin layer impressing the surface roughness, hydrophilicity and skin layer thickness [17]. Generally, membrane permeability enhances with the increment of the surface hydrophilicity and roughness and the decrement of the skin layer thickness. The hydrophilic CSGOs increase the attraction of water molecules on the membrane surface and improve the surface wettability, enhancing water permeability. Furthermore, the layered structure of CSGOs boosts the speed of water passage through the TFN membranes and increases their PWFs by creating new water channels (M. E. [5,16]; Y. [44,94]).

The surface roughness is considered as another parameter affected by the addition of the CSGOs within PEBA matrix. Higher PWFs are generally obtained for rougher membrane surfaces due to the increased surface area. As the third factor, the thickness of the skin layer specifies the mass transfer resistance so that more mass transfer occurs through a thinner active layer [17]. However, these conditions may not always be found concurrently. As a result, each abovementioned parameter can be determined depending on their effectiveness. For this reason, the PWF follows an increase to a maximum value of 0.1 wt% CSGO and a decrease to a minimum one at 1 wt% followed by another slight increase at 2 wt% (Fig. 7(B)). This trend, similar for all three pressures, can be respectively explained as follows; by incorporating CSGO nanosheets up to 0.1 wt% within PEBA, water permeability increases gradually insofar as a maximum PWF is obtained for TFNCSGO0.1. Referring to the AFM and SEM results for TFNCGO0.1, it is clear that the surface roughness and the PEBA layer thickness have decreased and increased, respectively. However, the PWF enhances due to the enhanced hydrophilicity of the TFN membrane prevailing over the effects described above. With the addition of more CSGOs to 1 wt%, the PWF experiences a descending trend. Here, the PWF has its minimum value despite the augmented hydrophilicity and roughness. The reason lies behind the accumulation of the nanofillers which block the water passageways. Although the higher agglomeration effect at 2 wt% has reduced the average surface roughness and the contact angle increment, an increase in water flux is seen. Probably, the reduced surface tension causes more PEBA solution to penetrate within the substrate so that a thinner active layer is formed.

3.5.2. Process duration

Membrane fouling is a phenomenon which mitigates the membrane performance and accelerates the membrane aging over time (F. A. A. [4, 63]). As a result, evaluating the membrane separation properties (permeate flux-rejection) during the processing time can be helpful to investigate the membrane antifouling property. Herein, the dye removal capability of the synthesized membranes was determined during 300 min to study the performance and antifouling properties of the membranes. For this purpose, nanofiltration tests were carried out for Malachite green (MG) dye at P = 2 bar and C = 30 mg/L for five specimens each accumulated per 60 min. The results are illustrated in Fig. 8 (A) and (B).

As observed in Fig. 8(A), the permeate flux of the TFN membranes follows a similar trend as their PWF, i.e. a maximum and a minimum value at 0.1 wt% and 1 wt% CSGO loading, respectively. The detailed interpretation of this behavior has been presented in §3.5.1. Furthermore, the average rejection factors (R%) of the TFN membranes are 98.54, 99.07, 99.63 and 99.46 for TFNCSGO0.1, TFNCSGO0.5, TFNCSGO1 and TFNCSGO2, respectively, which are higher than that of TFC one i.e. 97.9%, see Fig. 8(B). The abovementioned results are confirmed according to the absorption plot of the MG, typically shown for TFC, TFNCSGO0.1 and TFNCSGO1. However, a considerable change is not perceived in rejection despite permeation enhancement. In other words, it can be concluded that there is not any permeation-rejection (permeability-selectivity) trade-off [69].

Moreover, at similar pressure of 2 bar, the PWFs are higher than the permeate fluxes of the dye solution. This perception involves the deposition of dye molecules on the membrane surfaces and, thus, the fouling phenomenon. However, fouling is highly affected by the membrane surface charge, hydrophilicity and roughness, explained as follows: (1) similar charges of the surface and foulants result in repulsive electrostatic forces between them and, consequently, less fouling. Here, CSGO nanofillers have a positive charge due to the protonation of N-H groups of chitosan in acidic media as in our work (pH = 4.5). (2) The more the membrane hydrophilicity, the less the attachment of the foulants on the surface.

In our work, the improved hydrophilicity of the CSGO-PEBA/PES membranes diminishes the fouling. (3) The increased surface roughness provides suitable sites for the foulants to deposit. Hence, fouling increased with surface roughness (M. E. [5,16,17]; Y. [44]). As illustrated in Fig. 8(B) and (C), the slight decline of the permeate flux and rejection demonstrates the meliorated hydrophilicity and antifouling property of the CSGO-embedded TFN membranes.

Furthermore, the TFNCSGO membrane's performances are compared with other published works listed in Table 3. As observed, in spite of lower transmembrane pressure, CSGO/PEBA/PES TFN membranes show relatively good performance in terms of hydrophilicity, water permeability and dye rejection.

3.5.3. Feed concentration

In order to evaluate the effect of feed concentration on the membrane performance, the permeate flux and rejection behaviors were typically studied for the TFNCSGO0.1 membrane at C = 60 mg/L. The results are presented and compared with those obtained at C = 30 mg/L in Fig. 9 (A) and (B). As shown in Fig. 9(A), the permeate flux declines with the feed concentration since more MG dye accumulates on the membrane surface. Indeed, a barrier of dye molecules by which the accessibility of water molecules to the membrane surface is confined is formed in the vicinity of the membrane surface. Furthermore, the adsorption and transfer of MG molecules by the TFNCSGO0.1 membrane are reduced due to the enhanced hydrophilicity. In addition to permeate flux, the TFNCSGO0.1 membrane rejection factor was also studied. The experimental data illustrated in Fig. 9(B), show the rejection increment with the feed concentration for the first two hours of the test. However, the membrane fouling increases over time and decreases the membrane selectivity. As more fouling occurred normally at higher feed concentrations, lower rejections are obtained for C = 60 mg/L after 2 h [20].

4. Conclusion

Thin film nanocomposite membranes were prepared by incorporating a novel chitosan-aided graphene oxide (CSGO) nanomaterial within the selective layer at different loadings 0, 0.1, 0.5, 1 and 2 wt%. For this purpose, a skin layer of PEBAX®1657 was coated on PES ultraporous support. The membranes were then evaluated with respect to the structural characteristics via FTIR, XRD, FESEM, AFM and contact angle analyses. The FTIR results showed phase mixing within the MM top-layer as well as new strong hydrogen bonds formed between CSGO amine groups and the C═O groups of PA. These interactions between CSGO and PEBA enhanced the crystallinity of this segment, revealed by XRD. Moreover, due to the absence of CSGO characteristic peaks in the XRD pattern, one could conclude the well dispersion of monolayer CSGOs within the polymeric matrix, also confirmed by FESEM and AFM. On the other hand, based on contact angle results, the TFN membranes hydrophilicity enhanced due to the hydrophilic characteristics of CSGOs, which improves the membrane surface wettability. Furthermore, the performance of the membranes was investigated in terms of water permeability and rejection for separating MG dye from water. The results showed the highest permeate flux and rejection for TFNCSGO0.1 and TFNCSGO1, respectively. Also, the positive charge of CSGO nanofillers induced by the chitosan N-H groups as well as the membrane hydrophilicity, diminished fouling. As an overall conclusion, chitosan has succeeded in decorating the GO nanosheets' surface. Subsequently, the proper dispersion engineering within the MM layer led to achieve enhanced water permeation and antifouling properties of the CSGO-filled PEBA membranes.

CRediT authorship contribution statement

Seyyedeh Rahil Mousavi: Conceptualization, Methodology, Investigation, Writing – original draft. **Morteza Asghari:** Conceptualization, Methodology, Resources, Writing – review & editing, Supervision. **Niyaz Mohammad Mahmoodi:** Methodology, Resources, Writing – review & editing, Supervision. **Iman Salahshoori:** Review & editing.

Declaration of Competing Interest

The authors declare that they have no known competing financial interests or personal relationships that could have appeared to influence the work reported in this paper.

Data Availability

Data will be made available on request.

References

[1] H.R. Afshoun, M. Pourafshari Chenar, A.F. Ismail, Effect of coating method and feed pressure and temperature on CO_2/CH_4 gas separation performance of Pebax/PES composite membranes, J. Gas. Technol. (2018) *3*.
[2] A. Aghigh, V. Alizadeh, H.Y. Wong, M.S. Islam, N. Amin, M. Zaman, Recent advances in utilization of graphene for filtration and desalination of water: a review, Desalination 365 (2015) 389–397.
[3] F.H. Akhtar, M. Kumar, K.-V. Peinemann, Pebax® 1657/Graphene oxide composite membranes for improved water vapor separation, J. Membr. Sci. 525 (2017) 187–194.
[4] F.A.A. Ali, J. Alam, A.K. Shukla, M. Alhoshan, J.M. Khaled, W.A. Al-Masry, M. Alam, Graphene oxide-silver nanosheet-incorporated polyamide thin-film composite membranes for antifouling and antibacterial action against Escherichia coli and bovine serum albumin, J. Ind. Eng. Chem. 80 (2019) 227–238.
[5] M.E. Ali, L. Wang, X. Wang, X. Feng, Thin film composite membranes embedded with graphene oxide for water desalination, Desalination 386 (2016) 67–76.
[6] H.R. Amedi, M. Aghajani, Aminosilane-functionalized ZIF-8/PEBA mixed matrix membrane for gas separation application, Microporous Mesoporous Mater. 247 (2017) 124–135.

[7] Z. Amini, M. Asghari, Preparation and characterization of ultra-thin poly ether block amide/nanoclay nanocomposite membrane for gas separation, Appl. Clay Sci. 166 (2018) 230–241.

[8] F. Amirkhani, H.R. Harami, M. Asghari, CO_2/CH4 mixed gas separation using poly (ether-b-amide)-ZnO nanocomposite membranes: Experimental and molecular dynamics study, Polym. Test. 86 (2020), 106464.

[9] F. Amirkhani, M. Mosadegh, M. Asghari, M.J. Parnian, The beneficial impacts of functional groups of CNT on structure and gas separation properties of PEBA mixed matrix membranes, Polym. Test. 82 (2020), 106285.

[10] S.S. Amrei, M. Asghari, M. Esfahanian, Z. Zahraei, Highly selective CNT-coupled-GO-incorporated polydimethylsiloxane membrane for pervaporative membrane bioreactor ethanol production, J. Chem. Technol. Biotechnol. 95 (2020) 1604–1613.

[11] M. Asghari, M. Mosadegh, H.R. Harami, Supported PEBA-zeolite 13X nano-composite membranes for gas separation: Preparation, characterization and molecular dynamics simulation, Chem. Eng. Sci. 187 (2018) 67–78.

[12] M. Asghari, S. Saadatmandi, M. Afsari, Graphene oxide and its derivatives for gas separation membranes, ChemBioEng Rev. 8 (5) (2021) 490–516.

[13] M. Asghari, S. Saadatmandi, M.J. Parnian, Polypyrrole-aided surface decoration of graphene oxide nanosheets as fillers for poly (ether-b-amid) mixed matrix membranes to enhance CO_2 capture, Int. J. Energy Res. 45 (7) (2021) 10843–10857.

[14] M. Asghari, M. Sheikh, M. Afsari, M. Dehghani, Molecular simulation and experimental investigation of temperature effect on chitosan-nanosilica supported mixed matrix membranes for dehydration of ethanol via pervaporation, J. Mol. Liq. 246 (2017) 7–16.

[15] L. Bai, Y. Liu, A. Ding, N. Ren, G. Li, H. Liang, Fabrication and characterization of thin-film composite (TFC) nanofiltration membranes incorporated with cellulose nanocrystals (CNCs) for enhanced desalination performance and dye removal, Chem. Eng. J. 358 (2019) 1519–1528.

[16] R. Bi, Q. Zhang, R. Zhang, Y. Su, Z. Jiang, Thin film nanocomposite membranes incorporated with graphene quantum dots for high flux and antifouling property, J. Membr. Sci. 553 (2018) 17–24.

[17] H.-R. Chae, J. Lee, C.-H. Lee, I.-C. Kim, P.-K. Park, Graphene oxide-embedded thin-film composite reverse osmosis membrane with high flux, anti-biofouling, and chlorine resistance, J. Membr. Sci. 483 (2015) 128–135.

[18] J. Chen, Z. Zhang, H. Lu, Structure design and properties investigation of Bi_2O_2Se/graphene van der Waals heterojunction from first-principles study, Surf. Interfaces 33 (2022), 102289.

[19] J.H. Chen, Z.B. Su, J.P. Xu, L.J. Lin, X.F. Dong, Q. Peng, Y.J. Nie, Fabrication of PEBA/Cu 2 O mixed-matrix membranes and their application in pyridine recovery from aqueous solution, RSC Adv. 7 (37) (2017) 22936–22945.

[20] N. Cheshomi, M. Pakizeh, M. Namvar-Mahboub, Preparation and characterization of TiO2/Pebax/(PSf-PES) thin film nanocomposite membrane for humic acid removal from water, Polym. Adv. Technol. 29 (4) (2018) 1303–1312.

[21] A.-M. Croitoru, A. Ficai, D. Ficai, R. Trusca, G. Dolete, E. Andronescu, S. C. Turculet, Chitosan/graphene oxide nanocomposite membranes as adsorbents with applications in water purification, Materials 13 (7) (2020) 1687.

[22] Z. Dai, L. Ansaloni, L. Deng, Recent advances in multi-layer composite polymeric membranes for CO_2 separation: a review, Green. Energy Environ. (2016).

[23] G. Dong, J. Hou, J. Wang, Y. Zhang, V. Chen, J. Liu, Enhanced CO_2/N_2 separation by porous reduced graphene oxide/Pebax mixed matrix membranes, J. Membr. Sci. 520 (2016) 860–868.

[24] C.H. Du, X.Y. Zhang, C.J. Wu, Chitosan-modified graphene oxide as a modifier for improving the structure and performance of forward osmosis membranes, Polym. Adv. Technol. 31 (4) (2020) 807–816.

[25] A.S. Embaye, L. Martínez-Izquierdo, M. Malankowska, C. Téllez, J. Coronas, Poly (ether-block-amide) copolymer membranes in CO_2 separation applications, Energy Fuels 35 (21) (2021) 17085–17102.

[26] A. Erfani, M. Asghari, Comparison of micro-and nano-sized CuBTC particles on the CO_2/CH4 separation performance of PEBA mixed matrix membranes, J. Chem. Technol. Biotechnol. 95 (11) (2020) 2951–2963.

[27] A. Erfani, M. Asghari, Comparison of different MOF fillers on CO_2 removal performance of supported PEBA mixed matrix membranes, Greenh. Gases: Sci. Technol. 11 (1) (2021) 128–143.

[28] M.R. Esfahani, S.A. Aktij, Z. Dabaghian, M.D. Firouzjaei, A. Rahimpour, J. Eke, A. R. Esfahani, Nanocomposite membranes for water separation and purification: Fabrication, modification, and applications, Sep. Purif. Technol. (2018).

[29] L. Fan, C. Luo, X. Li, F. Lu, H. Qiu, M. Sun, Fabrication of novel magnetic chitosan grafted with graphene oxide to enhance adsorption properties for methyl blue, J. Hazard. Mater. 215 (2012) 272–279.

[30] L. Fan, C. Luo, M. Sun, X. Li, F. Lu, H. Qiu, Preparation of novel magnetic chitosan/graphene oxide composite as effective adsorbents toward methylene blue, Bioresour. Technol. 114 (2012) 703–706.

[31] L. Fan, C. Luo, M. Sun, H. Qiu, X. Li, Synthesis of magnetic β-cyclodextrin–chitosan/graphene oxide as nanoadsorbent and its application in dye adsorption and removal, Colloids Surf. B: Biointerfaces 103 (2013) 601–607.

[32] X. Fan, G. Wei, X. Lin, X. Wang, Z. Si, X. Zhang, W. Zhao, Reversible switching of interlayer exchange coupling through atomically thin VO2 via electronic state modulation, Matter 2 (6) (2020) 1582–1593.

[33] Y. Gao, M. Hu, B. Mi, Membrane surface modification with TiO_2–graphene oxide for enhanced photocatalytic performance, J. Membr. Sci. 455 (2014) 349–356.

[34] N. Ghaemi, P. Daraei, F.S. Akhlaghi, Polyethersulfone nanofiltration membrane embedded by chitosan nanoparticles: fabrication, characterization and performance in nitrate removal from water, Carbohydr. Polym. 191 (2018) 142–151.

[35] K. Gul, S. Sohni, M. Waqar, F. Ahmad, N.N. Norulaini, M.O. AK, Functionalization of magnetic chitosan with graphene oxide for removal of cationic and anionic dyes from aqueous solution, Carbohydr. Polym. 152 (2016) 520–531.

[36] S. Haeri, B. Ramezanzadeh, M. Asghari, A novel fabrication of a high performance SiO_2-graphene oxide (GO) nanohybrids: characterization of thermal properties of epoxy nanocomposites filled with SiO_2-GO nanohybrids, J. Colloid Interface Sci. 493 (2017) 111–122.

[37] H.M. Hegab, Y. Wimalasiri, M. Ginic-Markovic, L. Zou, Improving the fouling resistance of brackish water membranes via surface modification with graphene oxide functionalized chitosan, Desalination 365 (2015) 99–107.

[38] S.M. Hosseinifard, M.A. Aroon, B. Dahrazma, Application of PVDF/HDTMA-modified clinoptilolite nanocomposite membranes in removal of reactive dye from aqueous solution, Sep. Purif. Technol. 251 (2020), 117294.

[39] Z. Huang, J. Ding, X. Yang, H. Liu, P. Song, Y. Guo, W. Zhan, Highly efficient oxidation of propane at low temperature over a Pt-based catalyst by optimization support, Environ. Sci. Technol. 56 (*23*) (2022) 17278–17287.

[40] A. Jafari Sanjari, M. Asghari, A review on chitosan utilization in membrane synthesis, ChemBioEng Rev. 3 (3) (2016) 134–158.

[41] V. Jegatheesan, B.K. Pramanik, J. Chen, D. Navaratna, C.-Y. Chang, L. Shu, Treatment of textile wastewater with membrane bioreactor: a critical review, Bioresour. Technol. 204 (2016) 202–212.

[42] A. Jomekian, R.M. Behbahani, T. Mohammadi, A. Kargari, CO 2/CH 4 separation by high performance co-casted ZIF-8/Pebax 1657/PES mixed matrix membrane, J. Nat. Gas. Sci. Eng. 31 (2016) 562–574.

[43] G.-d Kang, Y.-m Cao, Development of antifouling reverse osmosis membranes for water treatment: a review, Water Res. 46 (3) (2012) 584–600.

[44] Y. Kang, M. Obaid, J. Jang, I.S. Kim, Sulfonated graphene oxide incorporated thin film nanocomposite nanofiltration membrane to enhance permeation and antifouling properties, Desalination 470 (2019), 114125.

[45] R. Kardani, M. Asghari, N.F. Hamedani, M. Afsari, Mesoporous copper zinc bimetallic imidazolate MOF as nanofiller to improve gas separation performance of PEBA-based membranes, J. Ind. Eng. Chem. 83 (2020) 100–110.

[46] R. Kardani, M. Asghari, T. Mohammadi, M. Afsari, Effects of nanofillers on the characteristics and performance of PEBA-based mixed matrix membranes, Rev. Chem. Eng. 34 (6) (2018) 797–836.

[47] R. Khan, I.U. Haq, H. Mao, A.-S. Zhang, L.-H. Xu, H.-G. Zhen, Z.-P. Zhao, Enhancing the pervaporation performance of PEBA/PVDF membrane by incorporating MAF-6 for the separation of phenol from its aqueous solution, Sep. Purif. Technol. 256 (2021), 117804.

[48] Y.H. Khan, A. Islam, A. Sarwar, N. Gull, S.M. Khan, M.A. Munawar, T. Jamil, Novel green nano composites films fabricated by indigenously synthesized graphene oxide and chitosan, Carbohydr. Polym. 146 (2016) 131–138.

[49] T. Kuilla, S. Bhadra, D. Yao, N.H. Kim, S. Bose, J.H. Lee, Recent advances in graphene based polymer composites, Prog. Polym. Sci. 35 (11) (2010) 1350–1375.

[50] S. Kumar, J. Koh, Physiochemical and optical properties of chitosan based graphene oxide bionanocomposite, Int. J. Biol. Macromol. 70 (2014) 559–564.

[51] G. Lai, W. Lau, P. Goh, A. Ismail, Y. Tan, C. Chong, S. Awad, Tailor-made thin film nanocomposite membrane incorporated with graphene oxide using novel interfacial polymerization technique for enhanced water separation, Chem. Eng. J. 344 (2018) 524–534.

[52] G. Lai, W. Lau, P. Goh, A. Ismail, N. Yusof, Y. Tan, Graphene oxide incorporated thin film nanocomposite nanofiltration membrane for enhanced salt removal performance, Desalination 387 (2016) 14–24.

[53] W.-J. Lau, A. Ismail, Polymeric nanofiltration membranes for textile dye wastewater treatment: preparation, performance evaluation, transport modelling, and fouling control—a review, Desalination 245 (1–3) (2009) 321–348.

[54] L. Liu, C. Li, C. Bao, Q. Jia, P. Xiao, X. Liu, Q. Zhang, Preparation and characterization of chitosan/graphene oxide composites for the adsorption of Au (III) and Pd (II), Talanta 93 (2012) 350–357.

[55] W. Liu, F. Huang, Y. Liao, J. Zhang, G. Ren, Z. Zhuang, C. Wang, Treatment of CrVI-Containing Mg(OH)2 Nanowaste, Angew. Chem. (Int. Ed.) 47 (*30*) (2008) 5619–5622.

[56] S.G. Lovineh, M. Asghari, G. Khanbabaei, CO_2 permeation through poly (amide-6-b-ethylene oxide)-nanosilica membranes, Appl. Surf. Sci. 318 (2014) 176–179.

[57] A. Mahmoudi, M. Asghari, V. Zargar, CO $_2$/CH_4 separation through a novel commercializable three-phase PEBA/PEG/NaX nanocomposite membrane, J. Ind. Eng. Chem. 23 (2015) 238–242.

[58] I. Makertihartha, Z. Rizki, M. Zunita, P. Dharmawijaya, Dyes removal from textile wastewater using graphene based nanofiltration, Pap. Presente AIP Conf. Proc. (2017).

[59] M. Mosadegh, F. Amirkhani, H.R. Harami, M. Asghari, M.J. Parnian, Effect of Nafion and APTEOS functionalization on mixed gas separation of PEBA-FAU membranes: experimental study and MD and GCMC simulations, Sep. Purif. Technol. 247 (2020), 116981.

[60] I. Munnawar, S.S. Iqbal, M.N. Anwar, M. Batool, S. Tariq, N. Faitma, T. Jamil, Synergistic effect of chitosan-zinc oxide hybrid nanoparticles on antibiofouling and water disinfection of mixed matrix polyethersulfone nanocomposite membranes, Carbohydr. Polym. 175 (2017) 661–670.

[61] S.P. Nunes, M.L. Sforça, K.-V. Peinemann, Dense hydrophilic composite membranes for ultrafiltration, J. Membr. Sci. 106 (1–2) (1995) 49–56.

[62] K.G. Pavithra, V. Jaikumar, Removal of colorants from wastewater: a review on sources and treatment strategies, J. Ind. Eng. Chem. 75 (2019) 1–19.

[63] S. Pourjafar, A. Rahimpour, M. Jahanshahi, Synthesis and characterization of PVA/PES thin film composite nanofiltration membrane modified with TiO_2

nanoparticles for better performance and surface properties, J. Ind. Eng. Chem. 18 (4) (2012) 1398–1405.
[64] N.S. Prasad, S. Moulik, S. Bohra, K.Y. Rani, S. Sridhar, Solvent resistant chitosan/poly (ether-block-amide) composite membranes for pervaporation of n-methyl-2-pyrrolidone/water mixtures, Carbohydr. Polym. 136 (2016) 1170–1181.
[65] D. Qadir, H. Mukhtar, L.K. Keong, Mixed matrix membranes for water purification applications, Sep. Purif. Rev. 46 (1) (2017) 62–80.
[66] M. Ramezanzadeh, M. Asghari, B. Ramezanzadeh, G. Bahlakeh, Fabrication of an efficient system for Zn ions removal from industrial wastewater based on graphene oxide nanosheets decorated with highly crystalline polyaniline nanofibers (GO-PANI): Experimental and ab initio quantum mechanics approaches, Chem. Eng. J. 337 (2018) 385–397.
[67] H. Riasat Harami, M. Asghari, A.H. Mohammadi, Magnetic nanoFe_2O_3–incorporated PEBA membranes for CO_2/CH_4 and CO_2/N_2 separation: Experimental study and grand canonical Monte Carlo and molecular dynamics simulations, Greenh. Gases: Sci. Technol. 9 (2) (2019) 306–330.
[68] J. Saadati, M. Pakizeh, Separation of oil/water emulsion using a new PSf/pebax/F-MWCNT nanocomposite membrane, J. Taiwan Inst. Chem. Eng. 71 (2017) 265–276.
[69] M. Safarpour, A. Khataee, V. Vatanpour, Thin film nanocomposite reverse osmosis membrane modified by reduced graphene oxide/TiO_2 with improved desalination performance, J. Membr. Sci. 489 (2015) 43–54.
[70] M. Safarpour, V. Vatanpour, A. Khataee, Preparation and characterization of graphene oxide/TiO2 blended PES nanofiltration membrane with improved antifouling and separation performance, Desalination 393 (2016) 65–78.
[71] E. Salehi, P. Daraei, A.A. Shamsabadi, A review on chitosan-based adsorptive membranes, Carbohydr. Polym. 152 (2016) 419–432.
[72] H. Salehi, M. Rastgar, A. Shakeri, Anti-fouling and high water permeable forward osmosis membrane fabricated via layer by layer assembly of chitosan/graphene oxide, Appl. Surf. Sci. 413 (2017) 99–108.
[73] S.F. Seyedpour, A. Rahimpour, H. Mohsenian, M.J. Taherzadeh, Low fouling ultrathin nanocomposite membranes for efficient removal of manganese, J. Membr. Sci. 549 (2018) 205–216.
[74] A. Shakeri, H. Salehi, M. Rastgar, Chitosan-based thin active layer membrane for forward osmosis desalination, Carbohydr. Polym. 174 (2017) 658–668.
[75] L. Shao, X. Chang, Y. Zhang, Y. Huang, Y. Yao, Z. Guo, Graphene oxide cross-linked chitosan nanocomposite membrane, Appl. Surf. Sci. 280 (2013) 989–992.
[76] P. Sharma, M.R. Das, Removal of a cationic dye from aqueous solution using graphene oxide nanosheets: investigation of adsorption parameters, J. Chem. Eng. Data 58 (1) (2013) 151–158.
[77] M. Sheikh, M. Asghari, M. Afsari, Effect of tiny amount of zinc oxide on morphological and thermal properties of nanocomposite PEBA thin films, Alex. Eng. J. 57 (4) (2018) 3661–3669.
[78] M. Shi, R. Wang, L. Li, N. Chen, P. Xiao, C. Yan, X. Yan, Redox-active polymer integrated with MXene for ultra-stable and fast aqueous proton storage, Adv. Funct. Mater. (2022) 2209777.
[79] M. Shi, H. Zhu, C. Chen, J. Jiang, L. Zhao, C. Yan, Synergistically coupling of graphene quantum dots with Zn-intercalated MnO_2 cathode for high-performance aqueous Zn-ion batteries, *Int. J. Miner. Metall. Mater.* 30 (1) (2023) 25–32.
[80] Y. Song, Y. Sun, M. Chen, P. Huang, T. Li, X. Zhang, K. Jiang, Efficient removal and fouling-resistant of anionic dyes by nanofiltration membrane with phosphorylated chitosan modified graphene oxide nanosheets incorporated selective layer, J. Water Process Eng. 34 (2020), 101086.
[81] S. Sun, P. Deng, C. Peng, H. Ji, L. Mao, L. Peng, Selenium-modified chitosan induces HepG2 cell apoptosis and differential protein analysis, Cancer Manag. Res. (2022) 3335–3345.
[82] N.A. Travlou, G.Z. Kyzas, N.K. Lazaridis, E.A. Deliyanni, Graphite oxide/chitosan composite for reactive dye removal, Chem. Eng. J. 217 (2013) 256–265.
[83] J. Wang, Y. Wang, Y. Zhang, A. Uliana, J. Zhu, J. Liu, B. Van der Bruggen, Zeolitic imidazolate framework/graphene oxide hybrid nanosheets functionalized thin film nanocomposite membrane for enhanced antimicrobial performance, ACS Appl. Mater. Interfaces 8 (38) (2016) 25508–25519.
[84] J. Wang, Y. Wang, J. Zhu, Y. Zhang, J. Liu, B. Van der Bruggen, Construction of TiO2@ graphene oxide incorporated antifouling nanofiltration membrane with elevated filtration performance, J. Membr. Sci. 533 (2017) 279–288.
[85] X. Wang, Y. Zhao, E. Tian, J. Li, Y. Ren, Graphene oxide-based polymeric membranes for water treatment, Adv. Mater. Interfaces 5 (15) (2018) 1701427.
[86] Y. Wang, T. Sun, L. Tong, Y. Gao, H. Zhang, Y. Zhang, S. Zhu, Non-free Fe dominated PMS activation for enhancing electro-Fenton efficiency in neutral wastewater, J. Electroanal. Chem. 928 (2023), 117062.
[87] Z. Wang, X. Liu, S. Ni, X. Zhuang, T. Lee, Nano zero-valent iron improves anammox activity by promoting the activity of quorum sensing system, Water Res. 202 (2021), 117491.
[88] K.C. Wong, P.S. Goh, T. Taniguchi, A.F. Ismail, K. Zahri, The role of geometrically different carbon-based fillers on the formation and gas separation performance of nanocomposite membrane, Carbon 149 (2019) 33–44.
[89] R. Wu, Y. Tan, F. Meng, Y. Zhang, Y. Huang, PVDF/MAF-4 composite membrane for high flux and scaling-resistant membrane distillation, Desalination 540 (2022), 116013.
[90] Z. Wu, H. Zhong, X. Yuan, H. Wang, L. Wang, X. Chen, Y. Wu, Adsorptive removal of methylene blue by rhamnolipid-functionalized graphene oxide from wastewater, Water Res. 67 (2014) 330–344.
[91] J. Xue, S. Wang, X. Han, Y. Wang, X. Hua, J. Li, Chitosan-functionalized graphene oxide for enhanced permeability and antifouling of ultrafiltration membranes, Chem. Eng. Technol. 41 (2) (2018) 270–277.
[92] Y. Yang, M. Zhao, L. Lai, Surface activity, micellization, and application of nano-surfactants—amphiphilic carbon dots, Carbon 202 (2023) 398–413.
[93] J. Yin, Fabrication and modification of nanocomposite membranes for enhanced water purification, Univ. Mo. –Columbia (2014).
[94] J. Yin, G. Zhu, B. Deng, Graphene oxide (GO) enhanced polyamide (PA) thin-film nanocomposite (TFN) membrane for water purification, Desalination 379 (2016) 93–101.
[95] L. Yu, Y. Zhang, B. Zhang, J. Liu, H. Zhang, C. Song, Preparation and characterization of HPEI-GO/PES ultrafiltration membrane with antifouling and antibacterial properties, J. Membr. Sci. 447 (2013) 452–462.
[96] V. Zargar, M. Asghari, M. Afsari, Gas separation properties of swelled nanocomposite chitosan membranes cross-linked by 3-aminopropyltriethoxysilane, Int. J. Environ. Sci. Technol. 16 (1) (2019) 37–46.
[97] V. Zargar, M. Asghari, A. Dashti, A review on chitin and chitosan polymers: structure, chemistry, solubility, derivatives, and applications, ChemBioEng Rev. 2 (3) (2015) 204–226.
[98] V. Zargar, M. Asghari, B. Rajaei, Synthesis and characterization of novel nanocomposite Chitosan membranes for ethanol dehydration, Int. J. Nano Dimens. 5 (5) (2014) 441–446.
[99] S. Zhang, M.H. Peh, Z. Thong, T.-S. Chung, Thin film interfacial cross-linking approach to fabricate a chitosan rejecting layer over poly (ether sulfone) support for heavy metal removal, Ind. Eng. Chem. Res. 54 (1) (2015) 472–479.
[100] Y. Zhang, H. Ruan, C. Guo, J. Liao, J. Shen, C. Gao, Thin-film nanocomposite reverse osmosis membranes with enhanced antibacterial resistance by incorporating p-aminophenol-modified graphene oxide, Sep. Purif. Technol. 234 (2020), 116017.
[101] C. Zhao, J. Xue, F. Ran, S. Sun, Modification of polyethersulfone membranes–a review of methods, Prog. Mater. Sci. 58 (1) (2013) 76–150.
[102] S. Zinadini, A.A. Zinatizadeh, M. Rahimi, V. Vatanpour, H. Zangeneh, Preparation of a novel antifouling mixed matrix PES membrane by embedding graphene oxide nanoplates, J. Membr. Sci. 453 (2014) 292–301.